SEMILEPTONIC DECAYS OF THE B-MESON

DAVID BRITTON
Physics Department, McGill University,
Montreal, Province of Quebec, H3A 2T8, Canada

(Representing the ARGUS Collaboration*)

ABSTRACT

Recent results on the semileptonic decay of B-mesons are reported from the ARGUS experiment, operating at the DORIS II e^+e^- storage ring at DESY. Two new measurements of the inclusive semileptonic branching ratio are presented which are in agreement with previous results and remain somewhat lower than theoretical predictions. One analysis, in particular, strives to reduce the model dependence by examining the inclusive lepton spectrum to low momenta, yielding a result of $10.9 \pm 0.6 \pm 0.4\%$. An examination of exclusive decays to D and D^* - mesons confirm that the inclusive rate is not saturated by these channels but the discrepancy is explained by two new measurements of a large $B \to D^{**}\ell\nu$ branching ratio of $4.0 \pm 0.6 \pm 0.2\%$ and $3.8 \pm 0.9 \pm 0.6\%$.

© D. Britton 1993

1. Introduction

There have been two points of inconsistency associated with the semileptonic decays of B-mesons. The first concerns the marginal discrepancy between the measured inclusive branching ratio and its theoretical prediction; the second is the fact that the inclusive branching ratio is nowhere near saturated by the observed exclusive decays into D and D^*-mesons.

Recent measurements of the inclusive rate yield values below about 11% from ARGUS,[1] CLEO,[2] CUSB,[3] and one measurement of 12% from Crystal Ball.[4] Theoretical estimates based upon a pure parton picture with inert spectator light quarks (see Figure 1) typically give values[5–7] of around 14% with a more recent work[8] estimating a branching ratio as low as (11.5-12)%. Any disagreement with the experimental branching ratio is, therefore, marginal and is further mitigated by a current suggestion[9] of corrections for non-perturbative effects where the dominant term is $\propto 1/M_q^2$ which leads to a reduction of up to 10% in the theoretical semileptonic branching ratio. It is also possible that non-spectator effects could be involved which would reduce the expected branching ratio. Figure 1 illustrates the possible w-exchange and annihilation diagrams that would dilute the relative importance of the semileptonic branching ratio. In addition, interference between internal and external spectator diagrams (see Figure 1) can occur when one of the light quarks from the w-decay is identical to the spectator quark.[6,10–12] Whilst non-spectator effects are expected to play a large role in D-meson decays, as indicated by the big difference between the charged and neutral D-lifetimes, the heavier mass of the b-quark is expected to reduce their importance in B-meson decays.[13]

The 1992 Particle Data Group[14] branching ratios for semileptonic B-meson decay to D and D^*-mesons account for only $(6.4 \pm 1.1)\%$ out of the average inclusive measurement of $(10.7 \pm 0.5)\%$. An indication that the remaining 3.3% may be explained by decays to the D^{**}-meson was published by CLEO[2] from fits to the inclusive lepton spectrum in which the D^{**} contribution was allowed to float. In contrast, the only theoretical model that explicitly includes a D^{**} contribution[15] suggests about 13% of semileptonic decays proceed via the D^{**}, which translates to a branching ratio of roughly 1.4%. However, this fraction depends on the ratio of D^*/D production which is related to the slope of the form factor in heavy quark effective theory[28] by the Bjorken sum rule.[29]

In this paper, two new analyses of the inclusive semileptonic branching ratio will be reported. The first of these makes a particular effort to escape from model dependent assumptions by utilising the low momentum region of the lepton spectrum. In addition, new values for the exclusive branching ratio into the D^*, and sum of $(D + D^*)$-mesons will be presented, along with two measurements of the semileptonic branching ratio into the D^{**}-meson. Following this introduction, the paper is divided into three sections, corresponding to three independent analyses, and then a final section which summarises the results and draws conclusions.

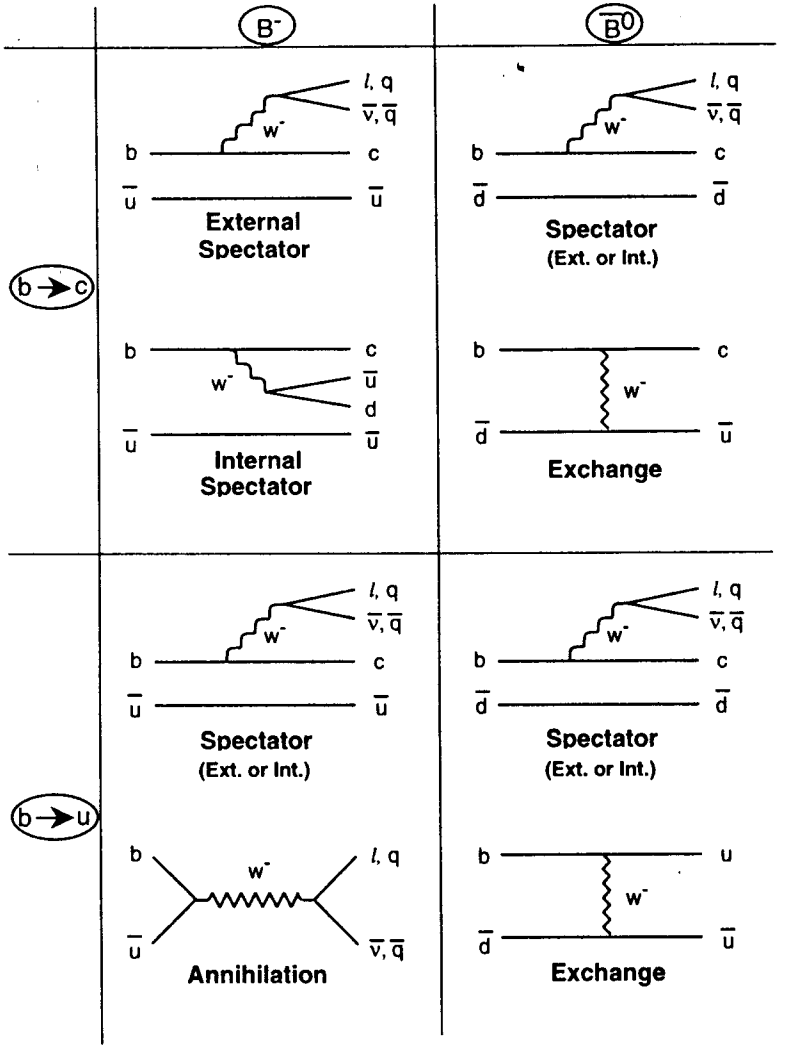

Figure 1: Diagrams for charged and neutral B-mesons decays via $b \to c$ and $b \to u$ transitions. See text for details.

2. Study of the Low Lepton Momentum Spectrum[a]

Introduction

The observed momentum spectrum of leptons accompanying the decay of B-mesons has two main components (see Figure 2): Primary leptons from semileptonic B-meson decays; and secondary (cascade) leptons from the semileptonic decay of charmed mesons produced in the decay of the B-mesons. The latter contribution is softer and contaminates the distribution up to about 1.4GeV/c. Previous measurements of the inclusive semileptonic branching ratio[1,2] rely heavily on models to describe the shape of the low momentum part of the lepton spectrum, either for the extrapolation of results found by fitting the region above 1.4GeV/c, or for determining the shape of the fitting function to be used below this momentum. The goal of the analysis described here is to extract and fit the primary lepton momentum spectrum to low momentum, and thus measure the inclusive semileptonic branching ratio in a largely model independent manner. The method employed is to tag one B-meson with an electron or muon of momentum greater than 1.4GeV/c (to try to ensure that it is indeed a primary lepton) and then to histogram the momentum spectrum of the oppositely charged electrons that accompany the decay of the other B-meson. That is, events containing a ($\mathrm{Tag}^{\pm}e^{\mp}$) pair are selected and, as illustrated in Figure 3, this requirement rejects secondary electrons from the cascade decay of the signal B-meson. Unfortunately, the following types of events represent backgrounds which must be subtracted before a pure primary lepton momentum distribution is revealed:

1. The cascade electron from the tagging B-meson is used as the signal electron.
2. The signal B-meson undergoes $B^0\overline{B}^0$ mixing and the cascade electron is selected as the signal.
3. A cascade lepton is used as the tag and the cascade lepton of the signal B-meson is selected.
4. The signal B-meson decays to a τ-meson which subsequently decays, giving an electron of the correct charge to be selected.
5. The signal B-meson decays to a D_s-meson which subsequently decays, giving an electron of the correct charge to be selected.
6. One, or both, of the ($\mathrm{Tag}^{\pm}e^{\mp}$) leptons come from the decay $B \rightarrow J/\psi X$ followed by $J/\psi \rightarrow \ell^+\ell^-$.
7. The signal electron comes from photon conversion where one electron is undetected.
8. Random ($\mathrm{Tag}^{\pm}e^{\mp}$) pairs from continuum events.
9. Fakes: events where one, or both, of the leptons is a misidentified hadron.

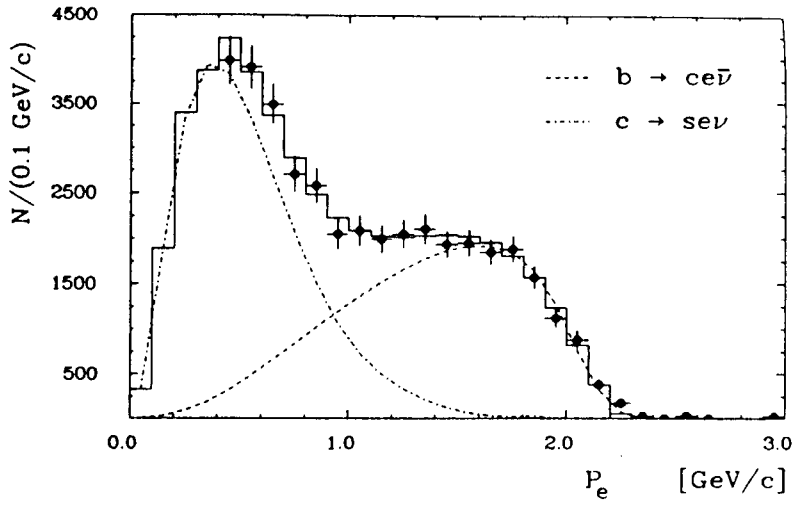

Figure 2: The inclusive lepton spectrum from B-decays. The dashed curve shows the primary lepton contribution, and the dot-dash curve the contribution from the cascade decays df charmed mesons.

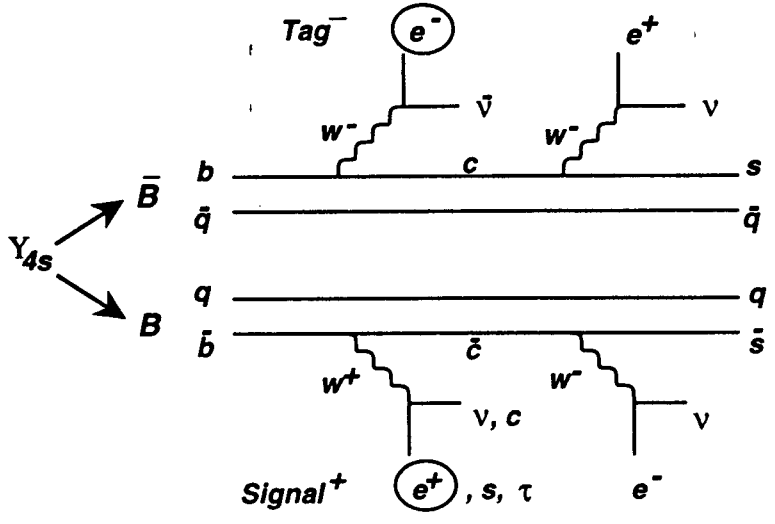

Figure 3: Leptons arising from the decay of a pair of B-mesons.

Data Analysis

The data used in this analysis consisted of 246pb^{-1} taken on the Υ_{4S} resonance, and 97pb^{-1} taken in the nearby continuum. The ARGUS detector and the lepton identification procedure have been described in detail elsewhere.[16] Events were selected containing a (Tag$^{\pm}e^{\mp}$) pair after a cut excluding e^+e^- pairs with an invariant mass of less than 0.1GeV was applied to suppress converted photons. The total multiplicity of the event, defined as $N_{tot} = N_{charged} + 0.5 * N_{\gamma}$, was required to be greater than five to suppress continuum events. Figure 4 shows the electron momentum distribution after the application of an important cut that required the cosine of the angle between the tag and the electron to be greater than zero. This cut removes 50% of the signal since the (Tag$^{\pm}e^{\mp}$) pair are essentially uncorrelated in direction. However, it suppresses 75% of the continuum background; 85% of the correlated background from cascade electrons (Background-1 above); and almost all of the background from J/ψ decays (Background-6). Figure 5 shows the same data after the subtraction of the scaled continuum contribution (Background-8), and of the faked leptons (Background-9) contribution. The primary electrons can be clearly seen above about 1GeV/c, whilst at low momenta the distribution is masked by the residual cascade electrons.

To subtract the contribution from Background-1 that remains after the $\cos\theta > 0$ requirement, the full angular distribution between the (Tag$^{\pm}e^{\mp}$) pair is used (shown in Figure 6). The primary (Tag$^{\pm}e^{\mp}$) pairs are uncorrelated and give rise to a constant distribution, whereas the pairs arising from Background-1 have an angular dependence which peaks at $cos\theta = -1$. The shape of the latter component is obtained from a Monte Carlo calculation using the model of ISGW[15] and turns out to be largely independent of the assumed D^{**} contribution. The data in Figure 6 corresponds to electrons with momentum between 0.6 and 0.8GeV/c, and was fitted with the two components from which the amplitude of Background-1 in the region $cos\theta > 0$ was obtained. This procedure was repeated for electrons in different momentum bins and the distribution shown in Figure 7 was obtained. This now may be directly subtracted from the signal spectrum to account completely for Background-1.

Backgrounds-2 and 3 also give rise to a component with the same cascade electron momentum distribution, but to perform the subtraction, the correct amplitude must be found. This may be obtained by looking at like-sign (Tag$^{\pm}e^{\pm}$) events (see Figure 8) where the electron momentum spectrum is complementary to the signal spectrum. That is, it contains a predominant contribution from cascade electrons but with some contamination from primary electrons *due to exactly the processes that cause Backgrounds-2 and 3*. The importance of this point is that it allows the normalisation to be calculated with minimal assumptions. The like-sign spectrum must first be corrected for continuum and fakes, as was the signal

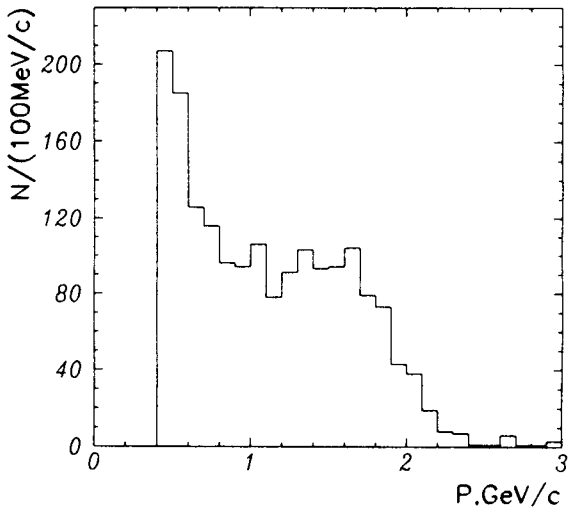

Figure 4: Electron momentum spectrum after a cut on the angle between the signal and tag: $\cos\theta_{tag,\ell} > 0$.

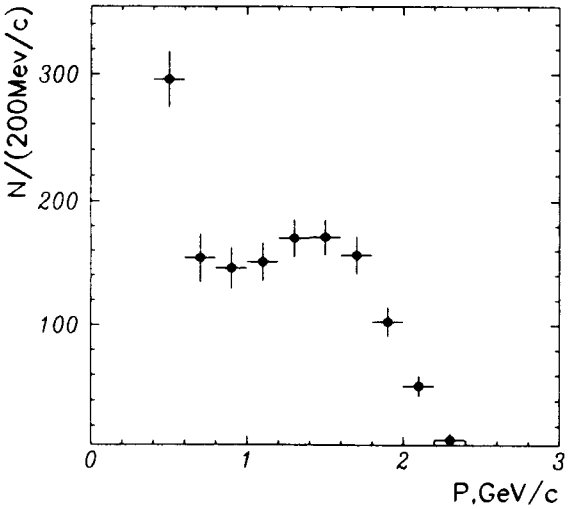

Figure 5: Electron momentum spectrum after subtraction of continuum and fake electron contributions.

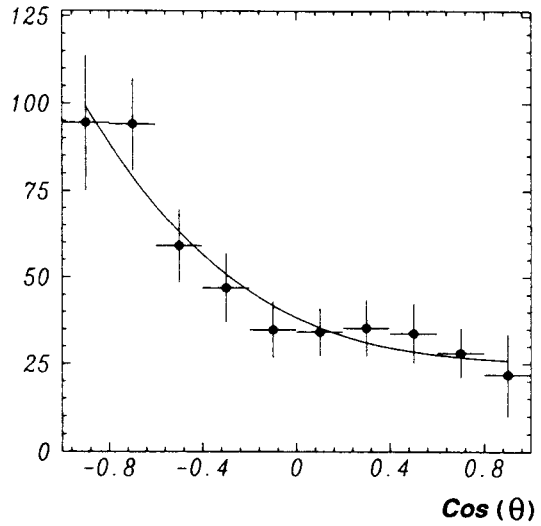

Figure 6: The angular distribution $\cos\theta_{tag,\ell}$ for electrons in the momentum range 0.6 — 0.8 GeV/c.

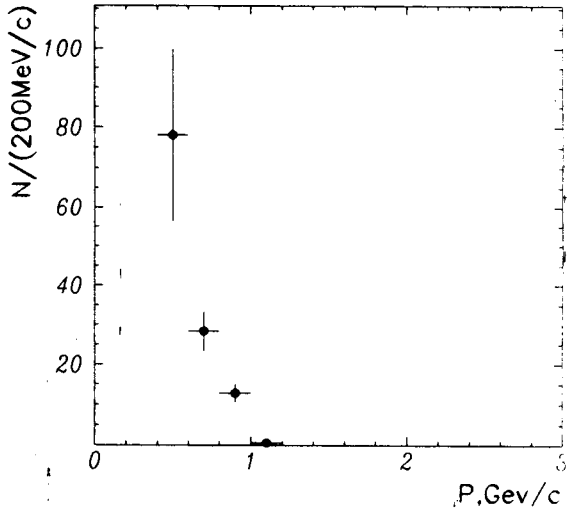

Figure 7: Momentum distribution of cascade electrons from Background-1 (see text).

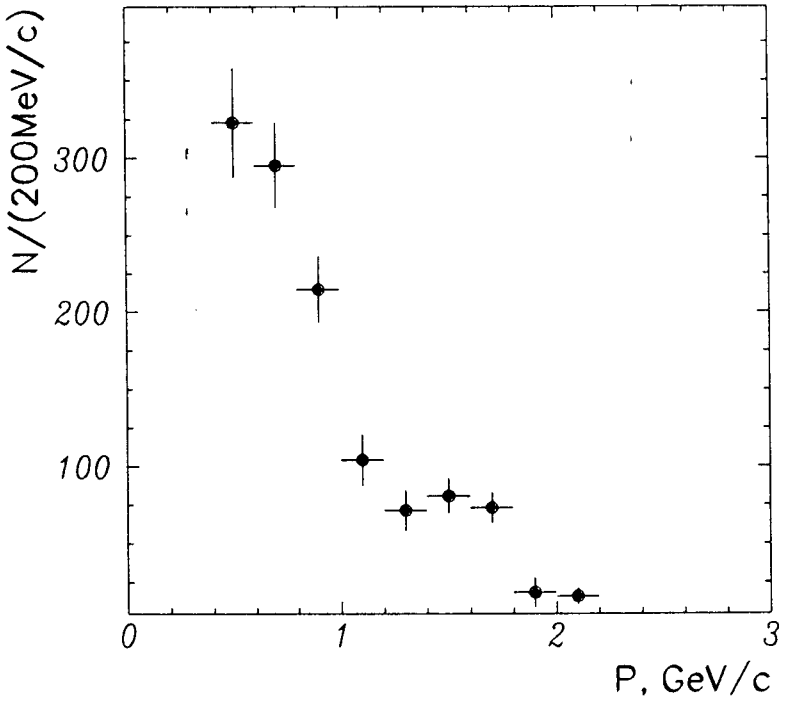

Figure 8: Lepton momentum distribution for like-sign tag-electron pairs.

spectrum, and then the normalisation factor is given by:

$$\frac{N^{uls}_{cascade}}{N^{ls}_{cascade}} = \frac{N^{ls}_{primary}}{N^{uls}_{primary}} = 0.097 \qquad (1)$$

where the superscripts *ls* and *uls* stand for *like-sign* and *unlike-sign* respectively, and where an electron is defined as primary (cascade) if it falls above (below) 1.4GeV/c. Implicit in this relationship is the assumption that the branching ratios of charged and neutral B-mesons into charmed mesons are identical. However, the systematic error on the final result includes the extreme case that the neutral B-meson decays only to D and D^*-mesons whilst the charged B-meson decay additionally to the D^{**}-meson. The left hand side of the above relationship can be measured directly from the data shown in Figures 5 and 8. The data in Figure 8 is then scaled by this factor and subtracted from Figure 5. This process also removes a known proportion of the primary lepton distribution which must be compensated in the final calculation of the branching ratio.

The contribution from background processes 4, 5 and 7 are simulated in a full Monte Carlo calculation and the resulting contributions to be subtracted from the signal are shown in Figure 9. The last of these may in principle be obtained directly from the data and work is presently underway to do so. The electron momentum spectrum after the subtraction of all backgrounds is shown in Figure 10, and the amplitudes and uncertainties of the various contributions are shown in Table 1.

Table 1: Signal and background summary for like-sign ($\mathrm{Tag}^{\pm}e^{\mp}$) events.

	Events before background subtraction	1779 ± 42
1	Cascade decays of tagging B-meson	$120 \pm 22 \pm 15$
2 + 3	$B^0\overline{B}^0$ mixing plus cascade electron tag	$112 \pm 14 \pm 20$
4	$B \to X\tau\nu_\tau,\ \tau \to e\nu\nu$	$39 \pm 1 \pm 3$
5	$B \to D_s X,\ D_s \to Xe\nu$	$60 \pm 2 \pm 11$
6	$B \to J/\psi,\ J/\psi \to \ell^+\ell^-$	$18 \pm 1 \pm 4$
7	Electrons from photon conversions	44 ± 10
8	Continuum events	$233 \pm 24 \pm 10$
9a	Hadrons misidentified as signal electrons	$84 \pm 2 \pm 5$
9b	Hadrons misidentified as tag leptons	$42 \pm 2 \pm 10$
	Events after background subtraction	$1027 \pm 56 \pm 29$

Results

The background subtracted electron spectrum must be corrected for Bremsstrahlung and for electron identification efficiency, resulting in the distribution shown in Figure 11. The solid line shows the result of a fit using the model of

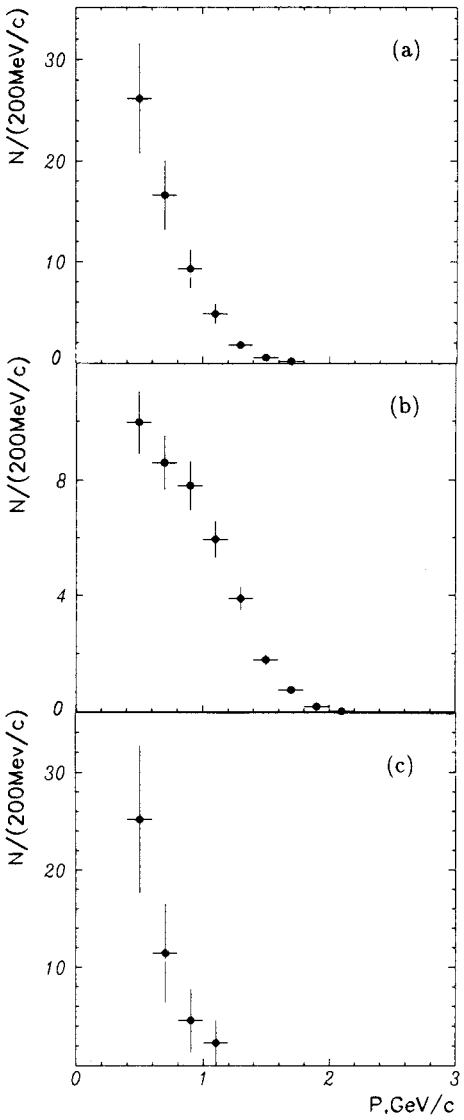

Figure 9: Momentum distribution of electrons from (a) D_s-decays; (b) τ-decays; and (c) converted photons.

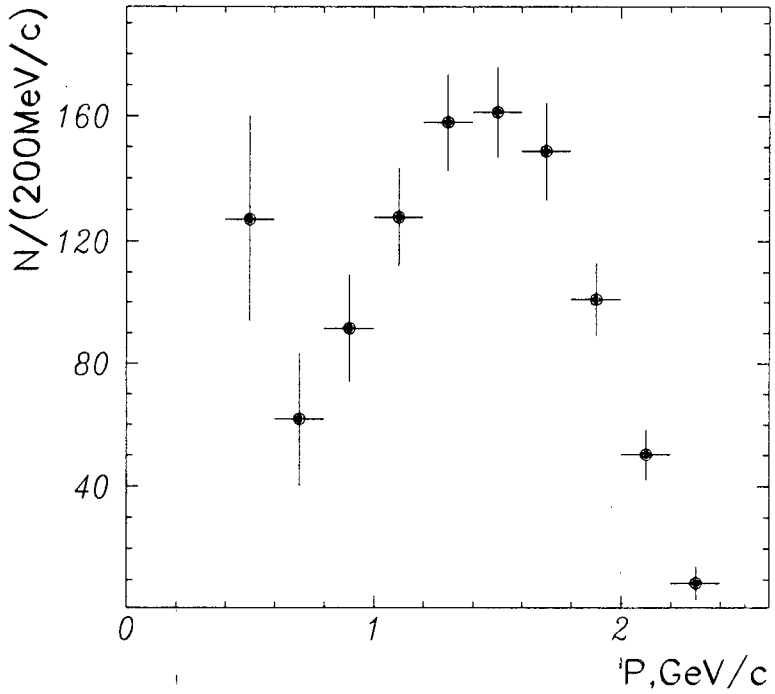

Figure 10: Momentum distribution of signal electrons after the subtraction of all backgrounds.

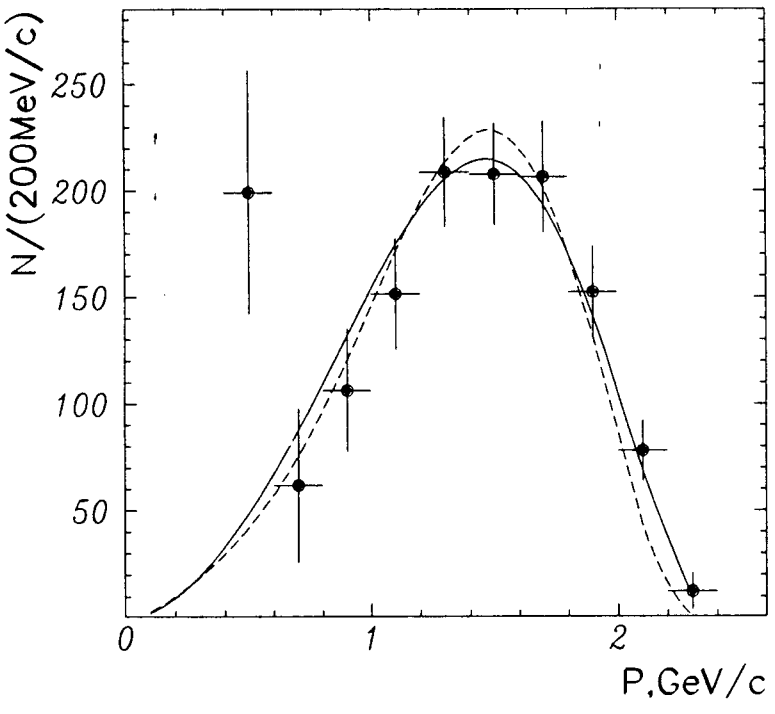

Figure 11: Momentum distribution of signal electrons after background subtraction and corrections for Bremsstrahlung and electron identification efficiency. Fits using the model of ISGW[15] and ACM[17] are shown by the solid and dashed curves respectively.

ISGW,[15] where the percentages of semileptonic decays to D, D^*, and D^{**}-mesons were fixed at 27%, 60%, and 13% respectively. The dashed line shows the result of a fit using the model of ACM[17] ($m_b = 4.95\text{GeV/c}^2$, $m_c = 1.56\text{GeV/c}^2$, $P_f = 0.30\text{GeV/c}$, $M_{sp} = 0.15\text{GeV/c}^2$). The resulting branching ratios are:

$$ISGW: \qquad BR(B \to Xe\nu) = (10.1 \pm 0.6 \pm 0.4)\% \quad . \tag{2}$$

$$ACM: \qquad BR(B \to Xe\nu) = (9.7 \pm 0.6 \pm 0.4)\% \quad . \tag{3}$$

However, the main thrust of this analysis was to minimise the model dependence, so just integrating the distribution and using either model to extrapolate below 0.4GeV/c, we obtain:

$$BR(B \to Xe\nu) = (10.9 \pm 0.6 \pm 0.4)\% \quad . \tag{4}$$

Unfortunately, the data point at lowest momentum in Figure 11 appears to be rather high. This could easily be a statistical fluctuation but since all the background contributions peak at low electron momentum it is possibly related to an incorrectly subtracted background or to an additional source of background. This is currently under investigation. Meanwhile, the effect of this point may be assessed by only integrating the data down to 0.6GeV/c and then extrapolating below this point according to the models. This gives $BR(B \to Xe\nu) = (9.7 \pm 0.6 \pm 0.4)\%$, but since there is no real justification for this procedure, the result quoted in Equation 4 will be taken as the preliminary result in the summary section of this paper.

3. Study of the Exclusive Contributions of the Inclusive Spectrum[b]

Introduction

The goal of this analysis was to see whether the inclusive lepton spectrum may be understood in terms of the exclusive decay modes to the D, D^*, and D^{**} charmed mesons, and to hadrons containing a u-quark. The technique is to try to separate the various channels by calculating the hadronic mass in the event, expressed in terms of the following 4-vectors:

$$M_X^2 = (P_B - P_\ell - P_\nu)^2 \quad . \tag{5}$$

In Υ_{4S} decays, the B-mesons are produced almost at rest ($\bar{p}_B = 0.35 GeV/c \simeq 0$). This assumption leads to:

$$M_X'^2 = M_B^2 + (P_\ell + P_\nu)^2 - 2E_B(E_\ell + E_\nu) \quad . \tag{6}$$

However, the mass M'_X calculated from this expression is only equal to the true hadronic mass in the event M_X under a second assumption that there are no missing particles in the event. This is because the neutrino momentum in Equation 6 is measured as the missing momentum in the event. The effect of these two assumptions may be investigated using a Monte Carlo simulation, as shown in Figure 12

for $B \to D^* \ell\nu$ decays. Ignoring detector resolution and assuming all particles are perfectly detected, then the shaded region shows the spread due to the non-zero momentum of the B-meson. The broad histogram shows the additional effect of missing particles. Figure 13 shows such distributions calculated for all the exclusive channels. The D and D^* contributions are indistinguishable and will be treated as a single component which is not a problem since the relative D^*/D branching ratio is known quite well[14] ($2.75 \pm^{1.00}_{0.75}$). In the calculation of these distributions the ISGW[15] model was assumed for the mass distributions of the D^{**} and X_u, where the latter are hadrons from $b \to u$ transitions with masses up to 1.7GeV/c^2. The distribution of missing momentum due to lost particles was verified by examining data with no leptons.

Data Analysis

From a data sample of 233pb^{-1}, events were selected with only one lepton of momentum greater than 1.2GeV/c which suppresses events where both B -mesons decayed semileptonically. The neutrino momentum vector was required to satisfy $|\cos\theta_\nu| < 0.9$ since beam-gas and $\gamma\gamma$ events tend to have missing momentum in the beam direction. The continuum was suppressed with standard cuts on the 2nd Fox-Wolfram moment, $H2 < 0.4$. The selected data then contained backgrounds from the following sources:

1. Residual continuum events: this contribution was subtracted by scaling the data taken in the continuum below the Υ_{4S} resonance.

2. Faked leptons: this component was subtracted using the well measured fake rates.

3. Leptons from J/ψ-decays, τ-decays, $\pi^0 \to \gamma e^+e^-$ decays, and $\gamma \to e^+e^-$ decays: these processes were simulated by Monte Carlo calculations and subtracted from the data.

4. Cascade leptons from the decay of charmed mesons: this component was not subtracted, but included in the fits as a free component.

The fits to the hadronic mass distributions thus had four components: X_u, $(D + D^*)$, D^{**}, and the cascade lepton contribution. The data were divided into seven bins of lepton momentum and the fits performed in the specific order indicated in Figure 14. If a particular contribution was expected to be small, it was fixed at a value extrapolated from fits to other momentum ranges. This is illustrated by the chart at the top of Figure 14. The results of the seven fits are shown in Figures 15 and 16. From the amplitudes found in these fits, the lepton momentum distributions of the three exclusive semileptonic channels are plotted in Figure 17, and the sum is shown in Figure 18. The error bars on the points in these figures come from the statistical error in the fits to the hadronic mass distribution, combined with a systematic error arising from the following:

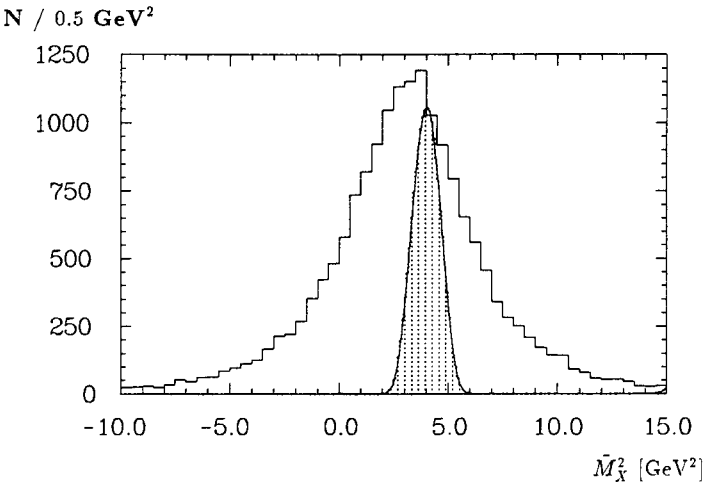

Figure 12: Monte Carlo simulation of hadronic mass measured in $B \to D^* \ell\nu$ decays. The dotted distribution shows the broadening due to the assumption $\bar{p}_B = 0$, and the histogram shows the additional effect of missing particles.

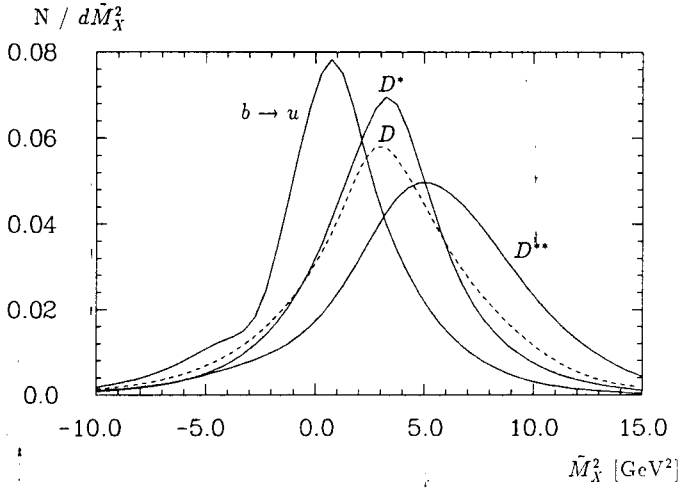

Figure 13: Monte Carlo generated distributions for the hadronic mass measured in $B \to (D, D^*, D^{**}, X_u)\ell\nu$ decays.

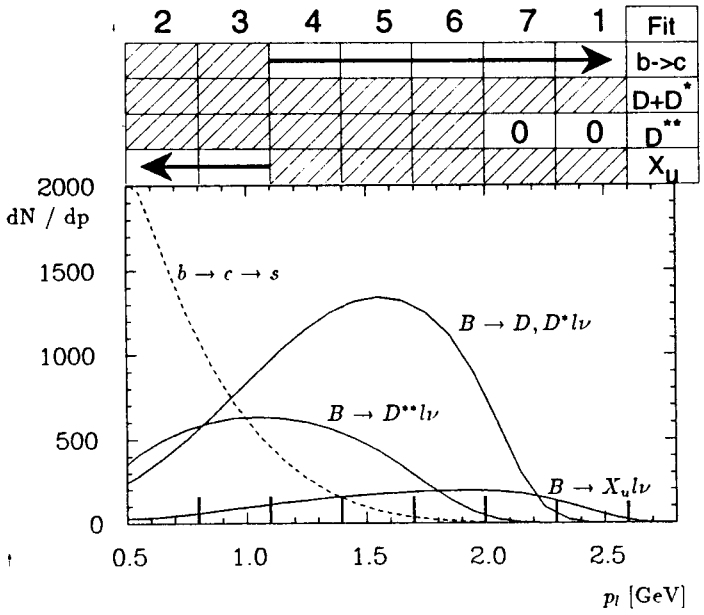

Figure 14: Contributions to the lepton momentum spectrum. The chart at the top illustrates the bins and the order in which the fits were performed. A shaded box indicates the particular component was free in the fit, otherwise it was fixed at a value extrapolated from previous fits.

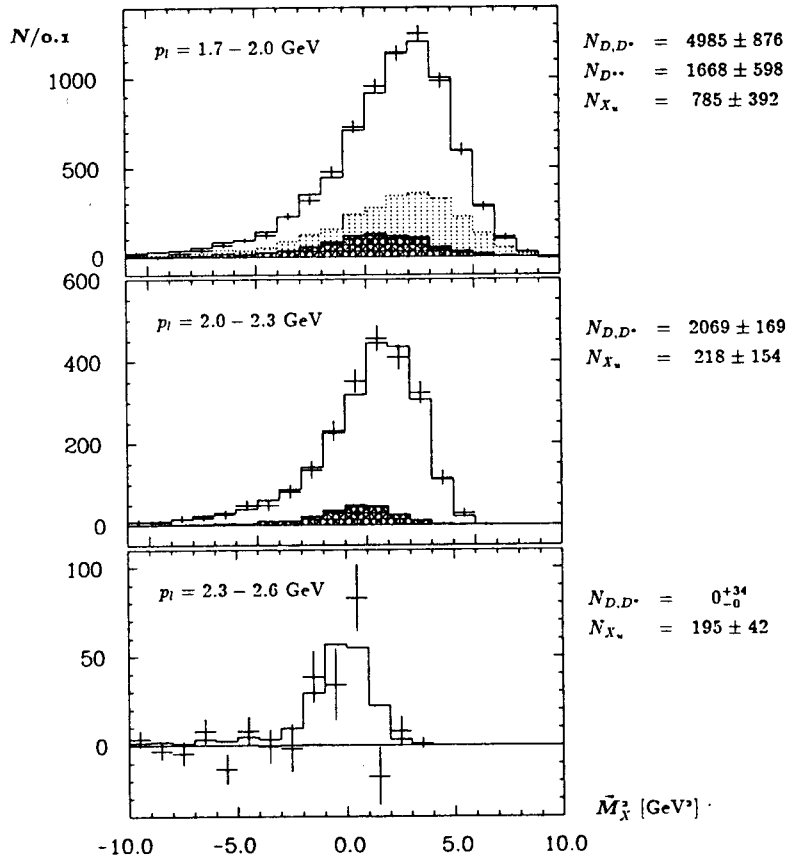

Figure 15: Results of fits to the hadronic mass distributions. The data is shown by the points with error bars and the histogram shows the results of the fits. The contributions from $(D + D^*)$ is shown by the unshaded region (except in the momentum bin 2.3 — 2.6 GeV/c where the only component is $B \rightarrow X_u$); the contribution from D^{**} is shown by the dotted region; the contribution from X_u by the double hatched region; and the contribution from $b \rightarrow c \rightarrow s$ background by the diagonally shaded areas.

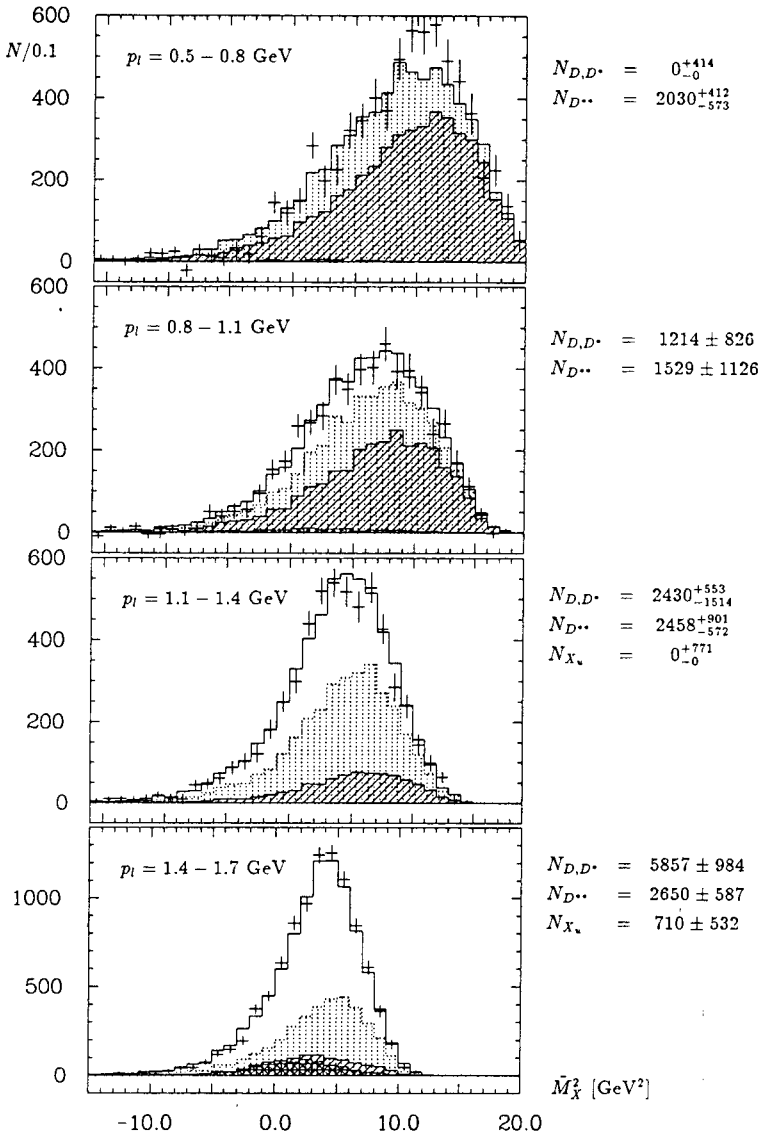

Figure 16: Results of fits to the hadronic mass distributions. See caption on the previous figure.

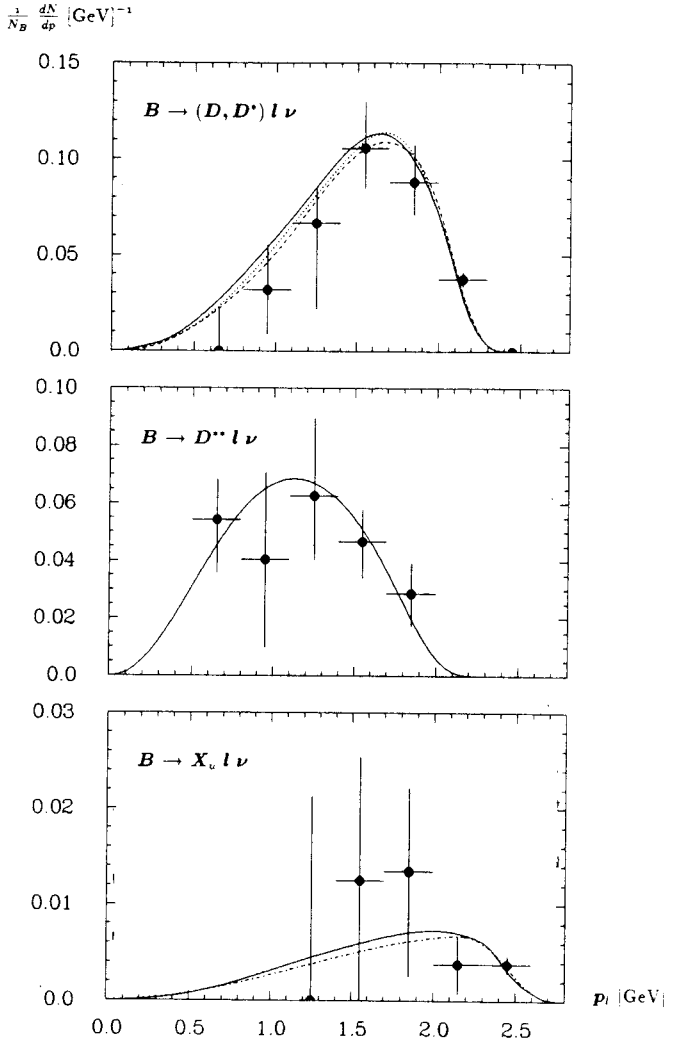

Figure 17: Lepton momentum spectrum for the exclusive B-meson decays, extracted from fits to the hadronic mass distributions. The solid, dashed, and dotted curves show fits using the models of WBS[18], ISGW[15], and KS[19] respectively.

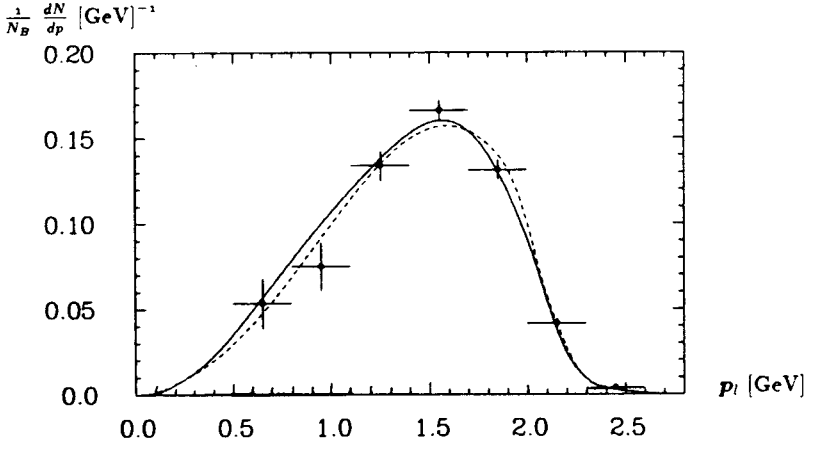

Figure 18: Sum of the exclusive lepton momentum distributions shown in Figure 17. The solid and dashed curves show fits using the models of ISGW[15] and ACM[17] respectively.

1. The background subtractions enumerated above.
2. The fitting process: the extrapolation of the fixed components, and the assumed D^*/D ratio.
3. The Monte Carlo calculations: different models for $B \to D^{(*)}\ell\nu$ decay (WBS,[18] KS,[19] ISGW[15]); the mass spectra used for $B \to D^{**}$ and $B \to X_u$ decays; missing momentum distributions due to lost particles; and the semileptonic branching ratio of the second B-meson.
4. Efficiencies: electron and muon identification; the cuts on H2 and upon $\cos\theta_\nu$; Bremsstrahlung; and momentum resolution.

Results

The solid curves in Figure 17 show fits using the model of WBS,[18] the dotted curve using KS,[19] and the dashed curve using ISGW.[15] In Figure 18 the solid curve is a fit to the inclusive spectrum using the model of ISGW[15] and the dashed curve uses ACM.[17] Table 2 contains the results of these fits where the values obtained from different models have been averaged and the spread incorporated in the systematic error.

Table 2: Branching ratios from fits to the lepton momentum spectra.

BR($B \to \{D + D^*\}\ell\nu$)	=	$6.02 \pm 0.52 \pm 0.35\%$
BR($B \to D^{**}\ell\nu$)	=	$3.99 \pm 0.60 \pm 0.20\%$
BR($B \to X_u\ell\nu$)	=	$0.49 \pm 0.11 \pm 0.04\%$
Sum of the above	=	$10.50 \pm 0.80 \pm 0.52\%$
BR($B \to X\ell\nu$)	=	$9.6 \pm 0.3 \pm 0.5\%$

It can be seen from Table 2 that the exclusive measurements saturate the inclusive branching ratio.

4. Study of Exclusive B-Meson Decays[c]

Introduction

The study of B-Meson decays into a $(D^{*+}\ell^-)$ state and its charged conjugate, can be used to determine both the $B \to D^*$ and the $B \to D^{**}$ exclusive semileptonic branching ratios. In addition, an analysis of the angular distributions leads to the observation of the effects of parity violation in the weak interaction. There are four processes identified in Table 3 that may result in a $(D^{*+}\ell^-)$ combination being identified as candidates in this analysis. The technique is to separate these components based upon their missing (or recoil) mass distributions defined as:

$$M^2_{miss} = (E_{beam} - E_{D^*} - E_\ell)^2 - (\vec{p}_{D^*} + \vec{p}_\ell)^2 \simeq M^2_\nu = 0. \qquad (7)$$

Table 3: Processes that give rise to $D^{*+}\ell^-$ pairs.

I	$\overline{B}^0 \to (D^{*+}\, l^-)\, \overline{\nu}_l$
II	$\overline{B}^0 \to D^{**+}\,(l^-, D^{*+})\,\overline{\nu}_l\,\pi^0 \qquad B^- \to D^{**0}\,(l^-, D^{*+})\,\overline{\nu}_l\,\pi^-$
III	$B_1 \to (l^-, D^{*+})\, X_1$ $B_2 \to (l^-, D^{*+})\, X_2$
IV	$e^+e^- \to c\bar{c} \to (D^{*+}\, l^-)\, X$

The approximation in Equation 7 is possible under the assumption that the momentum of the B-meson is zero, as in the previous analysis. Monte Carlo simulations of the missing mass squared distributions for the four processes noted in Table 3 are shown in Figure 19 where the area of each curve is normalised to unity for illustration.

Data Analysis

The data sample consisted of 233pb^{-1} collected on the Υ_{4S} resonance and for background studies, 105pb^{-1} from the nearby continuum. The D^* mesons were reconstructed in the decay $D^{*+} \to D^0\pi^+$ with $D^0 \to K^-\pi^+$ ($K\pi$-mode) or $D^0 \to K^-\pi^+\pi^+\pi^-$ ($K3\pi$-mode). The mass of the $K\pi$ or $K3\pi$ system was required to be within 60MeV/c^2 of the nominal D^0 mass, and the scaled momentum $x_p = P_{D^*}/\sqrt{E^2_{beam} - M^2_{D^*}}$ was restricted to be less than the maximum of 0.5 that is possible for decays from B-mesons. Figure 20 shows the reconstructed D^{*+} candidates for events where a lepton of momentum greater than 1 GeV/c and of the correct charge was identified. The distribution has been fitted with a Gaussian peak for the D^* signal and a background distribution obtained from Monte Carlo.* The same selection criteria may be applied to the continuum data which is shown in Figure 21; the resulting D^{*+} amplitudes will be used to constrain the continuum contribution (component IV in Table 3) in subsequent fits to the Υ_{4S} data. The data of Figure 20 was sub-divided into bins of M^2_{recoil} and the D^* mass peak was fitted in each bin. As a result, the M^2_{recoil} distributions shown in Figure 22 were obtained and fitted with the four components described in Table 3. The results of these fits are tabulated in Table 4.

*Depending on the D^0 decay channel there are typically five to ten types of combinatorics which contribute to the background. The relative amplitudes of these were obtained in fits to the data, and thus the background does not totally rely on the Monte Carlo.

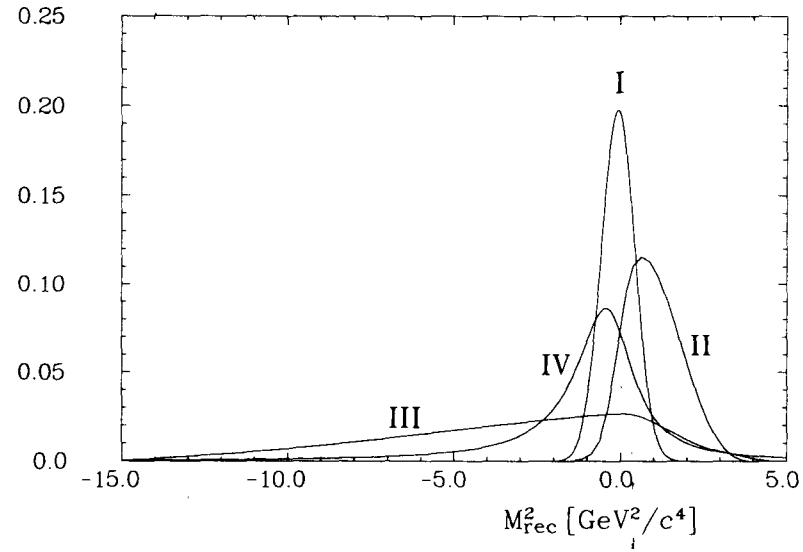

Figure 19: Recoil mass squared distributions for the four processes listed in Table 3. All curves are normalised to unit area.

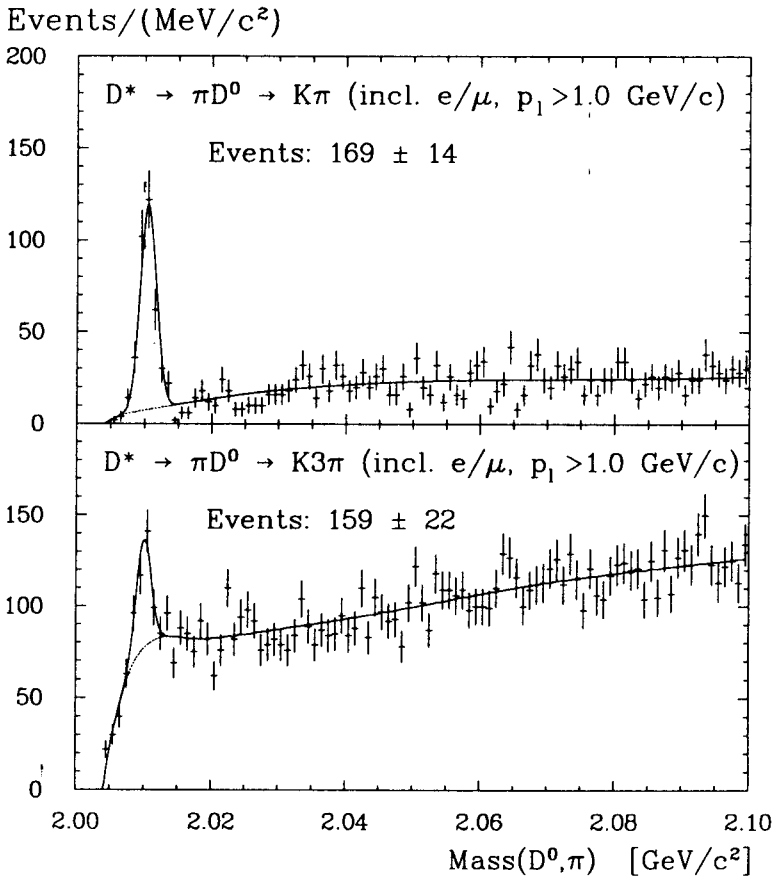

Figure 20: D^* mass plots for Υ_{4S} events containing a lepton with $p_\ell > 1.0$GeV/c: The upper plot shows events where the D^0 was reconstructed in the $K\pi$ channel, and the lower plot in the $K3\pi$ channel.

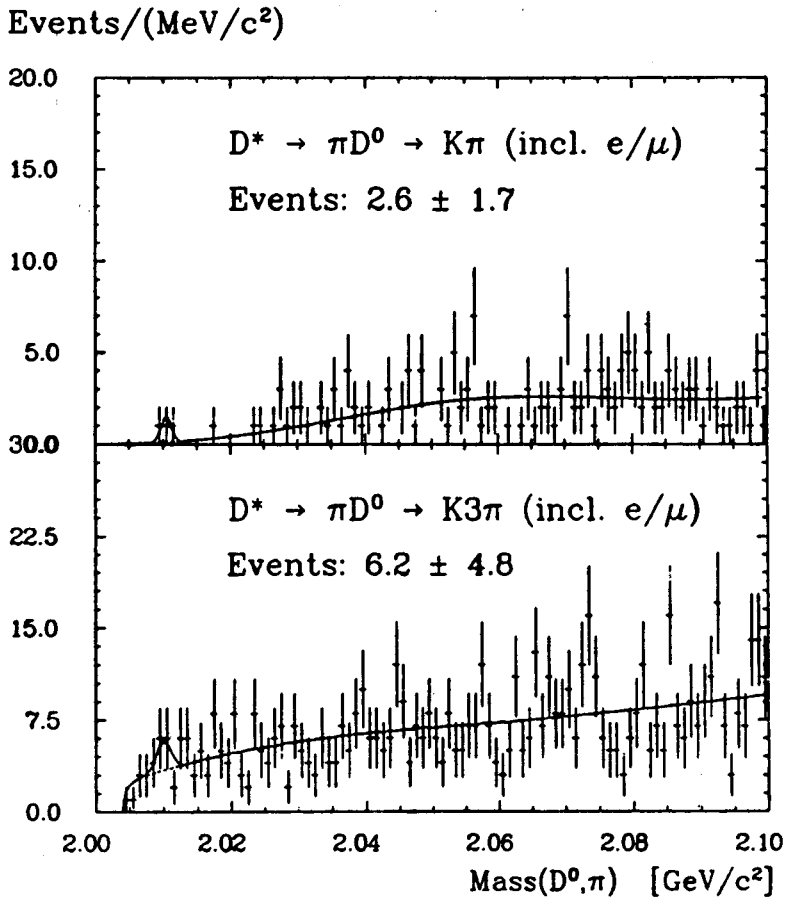

Figure 21: D^* mass plots for continuum events containing a lepton with $p_\ell > 1.0$GeV/c in analogy to Figure 20.

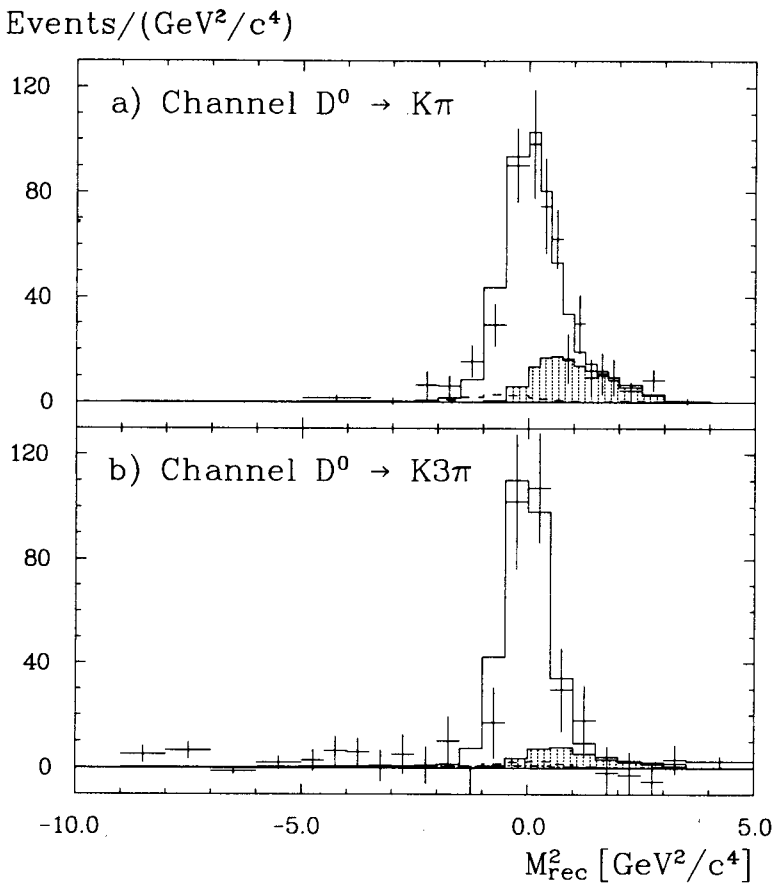

Figure 22: Recoil mass squared distributions. The points with error bars are the results of fits to the D^* signal shown in Figure 20. The histogram is the result of a fit using the four components listed in Table 3. The D^{**} and D^{*+} contributions are shown by the shaded and unshaded areas respectively; the other components are small.

The shaded distributions in Figure 22 show the fitted D^{**} contribution. As a cross-check, a D^{**} mass peak was observed by selecting D^* candidates with a M^2_{recoil} greater than zero and combining them with a charged pion. The combinatoric background was obtained by selecting events with a M^2_{recoil} less than zero. The observed signal of 30 ± 10 events shown in Figure 23 was in good agreement with the amplitude of $35 \pm 8 \pm 3$ events expected from the fits to the combined M^2_{recoil} distributions.

Table 4: Amplitudes found from fits to the M^2_{recoil} distribution for the four components listed in Table 3.

Process	Data Set		
	$K\pi$	$K3\pi$	$K\pi + K3\pi$
I	$114 \pm 13 \pm 6$	$124 \pm 23 \pm 9$	$235 \pm 24 \pm 11$
II	$34 \pm 9 \pm 2$	$21 \pm 13 \pm 4$	$63 \pm 15 \pm 6$
III	$8 \pm 4 \pm 5$	$14 \pm 10 \pm 6$	$16 \pm 7 \pm 8$
IV	$7 \pm 4 \pm 1$	$6 \pm 9 \pm 1$	$13 \pm 7 \pm 5$

Branching Ratio Results

The amplitudes in Table 4 lead to the preliminary result:

$$BR(\overline{B}^0 \to D^{**+}\ell^-\overline{\nu}) = 5.2 \pm 0.5 \pm 0.6\% \quad (8)$$

where the following branching ratios were assumed: $Br(D^* \to D^0\pi^+) = 66\%$, $Br(D^0 \to K^-\pi^+) = 3.71\%$, and $Br(D^0 \to K^-\pi^+\pi^+\pi^-) = 7.8\%$. From Table 4, the ratio of $D^*\ell$ pairs from $B \to D^{**}$ to $B \to D^*$ decays is calculated to be $0.27 \pm 0.08 \pm 0.03$. However, somewhat complex corrections must be made in order to convert this to a branching ratio. First of all, D^{**} decays involving a π^0 were not reconstructed in this analysis. Secondly, the D^{**} could come from the decay of the charged B-meson in addition to the neutral B-meson (process II in Table 3). Thirdly, the branching ratio of the D^{**} meson depends on the particular type of resonance[15] ($n^{2S+1}L_j = 1^1P_1, 1^3P_{1,2}, 2^1S_0, 2^3S_1$). Fourthly, the lepton identification efficiency is momentum dependent and since the leptons accompanying D^{**} mesons are softer than for D^* mesons, a correction must be made. With the following reasonable assumptions (the first simply represents the isospin Clebsch-Gordan coefficients):

$$BR(D_i^{**+} \to D^{*+}\pi^0) = \frac{1}{2} \cdot BR(D_i^{**0} \to D^{*+}\pi^-) = \frac{1}{3} \cdot BR(D_i^{**+} \to D^*X) \quad (9)$$

$$BR(B^- \to D_i^{**0}\ell^-\overline{\nu}_\ell) \simeq BR(\overline{B}^0 \to D_i^{**+}\ell^-\overline{\nu}_\ell) \quad (10)$$

$$N_{\overline{B}^-} = N_{\overline{B}^0} \quad (11)$$

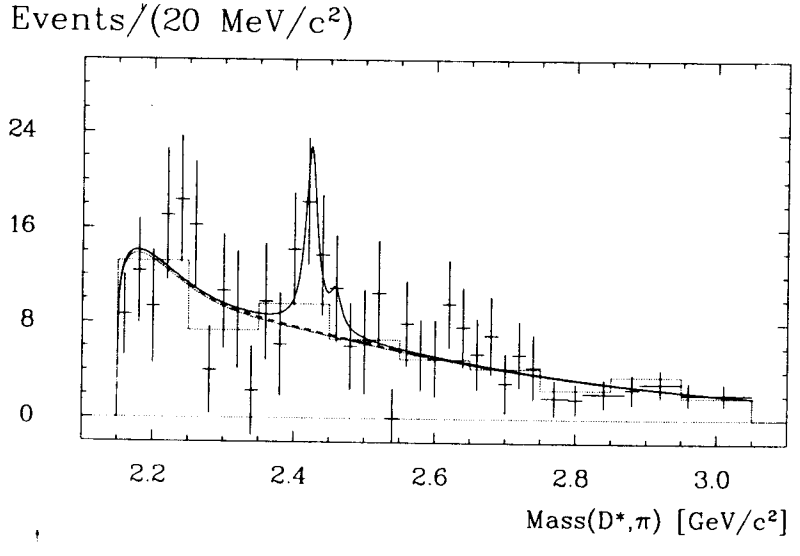

Figure 23: Mass plot of (D^*, π) combinations. The solid curve shows a fit including a D^{**} distribution and a combinatoric background.

the ratio of D^{**} to D^* events may be expressed as:

$$\frac{\#D^{**}}{\#D^*} = \frac{BR(\overline{B}^0 \to D_i^{**+}\ell^-\overline{\nu}_\ell)}{BR(\overline{B}^0 \to D_i^{*+}\ell^-\overline{\nu}_\ell)} \cdot \frac{\Sigma_i\{BR(\overline{B}^0 \to D_i^{**+}\ell^-\overline{\nu}_\ell) \cdot BR(D_i^{**+} \to D^*X) \cdot \epsilon_i\}}{\Sigma_i BR(\overline{B}^0 \to D_i^{**+}\ell^-\overline{\nu}_\ell)} \tag{12}$$

where the branching ratios for D^{**} type-i, and efficiency factors for lepton identification ϵ_i, are contained in Table 5. The branching ratio is finally calculated as:

$$BR(\overline{B}^0 \to D^{**+}\ell^-\overline{\nu}_\ell) = 3.8 \pm 0.9 \pm 0.6\% \quad . \tag{13}$$

This significant branching fraction to the D^{**} meson, when combined with the D and D^* contributions,[14] saturates the measured inclusive semileptonic branching ratio.

Table 5: Branching ratios and lepton identification efficiencies used to calculate the $B \to D^{**}$ semileptonic branching ratio.

i	D^{**}-type	Relative $BR(D_i^{**+} \to D^*X)$	Absolute $BR(\overline{B}^0 \to D_i^{**+}\ell^-\overline{\nu}_\ell)$ (ISGW[15])	ϵ_i (ISGW[15])
1	$D(1^1P_1)$	1	0.21	0.77
2	$D(1^3P_0)$	0	0.06	0.00
3	$D(1^3P_1)$	1	0.11	0.47
4	$D(1^3P_2)$	1/4	0.56	0.72
5	$D(2^1S_0)$	1	0.02	0.69
6	$D(2^3S_1)$	3/4	0.03	0.76

Parity Violation Effects

The decay sequence $\overline{B}^0 \to D^{**+}\ell^-\overline{\nu}$ followed by $D^{**+} \to D^0\pi^+$ is completely specified by q^2 and the three angles θ, θ^*, and χ, defined in Figure 24. Neglecting the lepton mass, the differential decay rate can be expressed as:

$$\frac{d^4\Gamma(q^2, \cos\theta, \cos\theta^*, \chi)}{dq^2\, d\cos\theta\, d\cos\theta^*\, d\chi} = \mathrm{Br}(D^{**+} \to D^0\pi^+)\frac{G^2}{(2\pi)^3}|V_{cb}|^2 \frac{q^2 p}{12M_{\overline{B}^0}^2} \times \left|\Sigma_\lambda\, d^1_{0,\lambda}(\theta^*) \cdot d^1_{\lambda,1}(\theta) \cdot e^{-i(\lambda+1)\chi} \cdot H_\lambda(q^2)\right|^2 \tag{14}$$

where p is the D^{**+} -momentum in the B rest frame and $H_\lambda(q^2)$ are the helicity form factors. Since the charmed quark in these decays is produced predominantly with negative helicity in the Standard Model, a forward-backward asymmetry (A_{FB}) is expected, defined in terms of the angle θ as:

$$A_{FB} = \frac{3}{4} \cdot \frac{\Gamma^- - \Gamma^+}{\Gamma} = \frac{\int_{-1}^{0} d\Gamma(\cos\theta) - \int_{0}^{+1} d\Gamma(\cos\theta)}{\int_{-1}^{+1} d\Gamma(\cos\theta)} \quad . \tag{15}$$

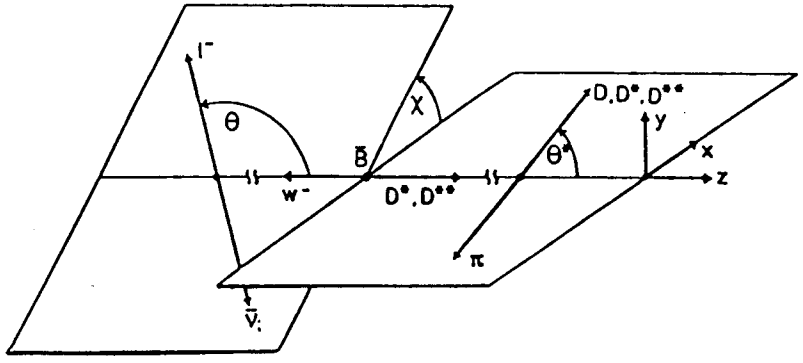

Figure 24: Definitions of the angles θ, θ^*, and χ.

The shape of the $\cos\theta$ distribution is given by:

$$\frac{d\Gamma(\cos\theta)}{d\cos\theta} \propto 2 + \alpha\sin^2\theta - \frac{4}{3}A_{FB}(3+\alpha)\cdot\cos\theta \qquad (16)$$

where the parameter α describes the $D^{*(*)}$ polarisation and may be extracted from the distribution of the angle θ^*:

$$\frac{d\Gamma(\cos\theta^*)}{d\cos\theta^*} \propto 1 + \alpha\cos^2\theta^* \quad . \qquad (17)$$

The distributions of θ, θ^*, M^2_{recoil}, and q^2 are produced by requiring that the momenta and energies of the D^{*+} and the ℓ^- be consistent with the presumed decay of a $\overline{B}^0$ meson. Specifically, the neutrino energy $E_{\overline{\nu}} = E_{beam} - E_{D^{*+}} - E_{\ell^-}$ must be positive, and the neutrino momentum $p_{\overline{\nu}} = E_{\overline{\nu}}$, together with the known $p_{\overline{B}^0} = \sqrt{E^2_{beam} - M^2_{\overline{B}^0}}$ and $p_{D^{*+}\ell^-} = |\vec{p}_{D^{*+}} + \vec{p}_{\ell^-}|$, must be consistent with momentum conservation, forming a closed momentum triangle. These conditions are satisfied only for $D^{*+}\,\ell^-$ pairs with $M^2_{rec} \approx 0$, and therefore automatically selects the decay $\overline{B}^0 \to D^{*+}\,\ell^-\,\overline{\nu}$, whilst considerably reducing the background. Figure 25 shows the $\cos\theta$, $\cos\theta^*$, q^2, and M^2_{rec} distributions obtained under these conditions without the application of efficiency corrections. The strong fall-off in the $\cos\theta$ spectrum as it approaches $+1$ is due to the cut on the lepton momentum, $p_l > 1\,\mathrm{GeV}/c$. The four distributions in Figure 25 are fitted simultaneously to the predictions of various theoretical models[15,18,19,24–26] for the process $\overline{B}^0 \to D^{*+}\,\ell^-\,\overline{\nu}$ and to the model of GISW[15] for $\overline{B}^0 \to D^{**}\,\ell^-\,\overline{\nu}$. To determine the forward-backward asymmetry A_{FB} and the polarization parameter α, the normalizations of the three invariant form factors in each model (which are related to the helicity form factors in Equation 14) are included in the fits as free parameters. The background rates in the $\cos\theta$, $\cos\theta^*$, and q^2 distributions due to processes II, III, and IV in Table 3 are determined from the M^2_{rec} spectrum. Finally, A_{FB} and α are calculated by inserting the fitted normalizations of the invariant form factors into Equation 14. A check was made to demonstrate that this procedure is not biased by the model used for the form factors. The method has the advantage that the values determined for A_{FB} and α are independent of the cut on the lepton momentum. The simultaneous fit makes maximal use of the available information and yields

$$\alpha = 1.12 \pm 0.39 \pm 0.19 \qquad (18)$$

$$A_{FB} = 0.20 \pm 0.08 \pm 0.06 \quad . \qquad (19)$$

The result for α is in good agreement with previous measurements from ARGUS[20] ($\alpha = 0.7 \pm 0.9$) and CLEO[21] ($\alpha = 1.21 \pm 0.48 \pm 0.19$). This first† measurement of A_{FB} is consistent with most theoretical estimates from form factor models.[15,18,19,22–25] QCD sum rules,[26] and heavy quark effective theory.[27]

†CLEO also announced a result for $A_{FB} = 0.14 \pm 0.06 \pm 0.03$ at this conference. See contribution from A. Freyberger.

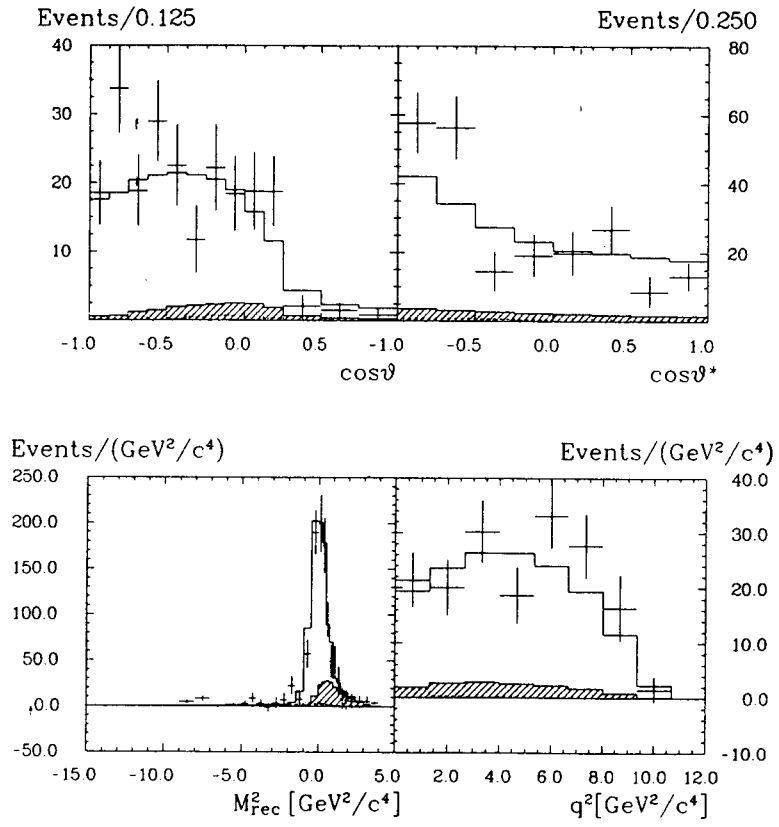

Figure 25: The measured $\cos\theta$, $\cos\theta^*$, M^2_{recoil}, and q^2 distributions, uncorrected for efficiency. The solid line histograms are the fitted sum of the Monte Carlo distributions expected for processes I — IV. The shaded histograms show the D^{**} contribution.

5. Summary of Branching Ratio Results, and Conclusions

All the semileptonic B-meson branching ratios reported in this paper are summarised in Table 6, along with previous world averages from the PDG[14] and other recent results not contained therein. For the sake of clarity and comparison, all the uncertainties have been added in quadrature; see the appropriate reference for the correct breakdown. All ARGUS results are preliminary.

Table 6: Summary of inclusive and exclusive B-meson semileptonic branching ratios.

Decay	BR %	Reference
$B \to Xe\nu$	10.7 ± 0.5	PDG[14]
	10.8 ± 0.6	CLEO[2]
	10.9 ± 0.7	Section-2
	10.5 ± 0.9	Section-3
	9.6 ± 0.6	Section-3
$B \to D\ell\nu$	1.7 ± 0.5	PDG[14]
$B \to D^*\ell\nu$	4.7 ± 0.9	PDG[14]
	5.2 ± 0.8	Section-4
$B \to (D + D^*)\ell\nu$	6.4 ± 1.1	PDG[14]
	6.0 ± 0.6	Section-3
$B \to D^{**}\ell\nu$	~ 1.4	Theory[15]
	~ 3.4	CLEO[2]
	4.0 ± 0.6	Section-3
	3.8 ± 1.1	Section-4

Three significant conclusions may be drawn from these results:

- The inclusive semileptonic branching fraction remains consistently less than the 12% that can be elegantly accommodated by the pure spectator models. This hints at non-spectator effects or the importance of the non-perturbative corrections as were discussed in the introduction.
- The exclusive branching fractions to D and D^* mesons are in good agreement with previous values and do not saturate the inclusive measurement.
- There is clearly a large D^{**} contribution. This is not in agreement with any model, but makes the sum of the exclusive branching ratios consistent with the inclusive measurement.

* The current members of the ARGUS collaboration are: H. Albrecht, H. Ehrlichmann, T. Hamacher, R. Hofmann, T. Kirchoff, A. Nau, S. Nowak, H. Schröder, H. Schulz, M. Walter, R. Wurth, (DESY, Germany), R. Appuhn, C. Hast, H. Kolanoski, A. Lange, A. Lindner, R. Mankel, M. Schieber, T. Siegmund, B. Spaan, H. Thurn, D. Töpfer, A. Walther, D. Wegener (Universität Dortmund, Germany), M. Paulini, K. Reim, H. Wegener, (Universität Erlangen-Nürnberg, Germany), R. Mundt, T. Oest, R. Reiner, W. Schmidt-Parzefall, (Universität Hamburg, Germany), W. Funk, J. Stiewe, S. Werner, (Universität Heidelberg, Germany), K. Ehret, W. Hofmann, A. Hupper, S. Khan, K. T. Knöpfle, J. Spengler, (MPI, Heidelberg, Germany), D. I. Britton, C. E. K. Charlesworth, K. W. Edwards, E. Hyatt, H. Kapitza, P. Krieger, D. B. MacFarlane, P. M. Patel, J. D. Prentice, P. Saull, K. Tzamariudaki, R. G. Van de Water, T.-S. Yoon, (IPP, Canada), D. Reßing, M. Schmidtler, M. Schneider, K. R. Schubert, K. Strahl, J. Tamminga, R. Waldi, S. Weseler, (Universität Karlsruhe, Germany), G. Kernel, P. Križan, E. Križnič, T. Podobnik, T. Živko, (Univerza v Ljubljani, Slovenia), H. I. Cronström, L. Jönsson, (University of Lund, Sweden), V. Balagura, I. Belyaev, M. Danilov, A. Droutskoy, A. Golutvin, I. Gorelov, G. Kostina, V. Lubimov, P. Murat, P. Pakhlov, F. Ratnikov, S. Semenov, V. Shibaev, V. Soloshenko, I. Tichomirov, Yu. Zaitsev, (ITEP, Moscow, Russia).
[a] Thesis work of G. Kostina, ITEP.
[b] Thesis work of T. Oest, University of Hamburg.
[c] Thesis work of K. Reim, University of Erlangen.

References

1. H. Albrecht et al.,(ARGUS), Phys. Lett. **B249** 359 (1990).
2. S. Henderson et al.,(CLEO), Phys. Rev. **D45** 2212 (1992).
3. C. Yanagisawa et al.,(CUSB), Phys. Rev. Lett. **66** 2436 (1991).
4. K. Wachs et al.,(CBALL), Z. Phys. **C42** 33 (1989).
5. J. Leveille, Universtiy of Michigan preprint UM-HE 81-18 (1981).
6. R. Rückl, Habilitationsschrift, Munich (1983).
7. J. Cortes et al., Phys. Rev. **D25** 188 (1982).
8. G. Altarelli and S. Petrarca, Phys. Lett. **B261** 303 (1991).
9. I. Bigi et al., Fermilab preprint PUB-92/158-T (1992).
10. A. Buras et al., Nucl. Phys. **B268** 16 (1986).
11. M. Shifman, in *Lepton and Photon Interactions*, Proceedings of the 1987 Lepton-Photon Conference, Hamburg, Germany. Edited by R. Rückl and W. Bartel, (Nucl. Phys. B(PRoc Suppl.) **3**, 289 (1988).
12. I. Bigi, in *Proceedings of the International Symposium on Heavy Quark Physics*, Cornell University, Ithaca, New York, 1989, edited by P.S. Drell and D.L. Rubin, AIP Conf. PRoc. No. 196 p.18.
13. I. Bigi and B. Stech, in *Proceedings of the Workshop on High Sensitivity Beauty Physics*, Batavia, Illinois, 1987, edited by A. Slaughter, N. Lockyer, and M. Schmidt.
14. Particle Data Group: Review of Particle Properties, Phys. Rev. **D45** (1992).
15. N. Isgur et al., Phys. Rev. **D39** 799 (1989).
16. H. Albrecht et al.,(ARGUS), Nucl. Instr. Meth. **A275** 1 (1989).
17. G. Altarelli et al., Nucl. Phys. **B208** 365 (1982).
18. M. Wirbel et al., Z. Phys. **C29** 637 (1985).
19. J. Körner and G. Schuler, Z. Phys. **C38** 511 (1988).
20. H. Albrecht et al., Phys. Lett. **B219** 121 (1989).
21. D. Bortoletto, Syracuse Univ. **PhD thesis,** (unpublished) (1989).
22. M. Suzuki, Nucl. Phys. **B258** 553 (1985).
23. F. Schöberl, H. Pietschmann, Europhys. Lett. **2** 583 (1986).
24. K. Hagiwara, A.D. Martin, M.F. Wade, Nucl. Phys. **B327** 569 (1989).
25. J. M. Cline,W.F.Palmer, G.Kramer, Phys. Rev. **D40** 793 (1989).
26. P. Ball, HD-THEP-92-25 (1992), to appear in Moriond Proceedings '92.
27. S. Balk, F. Hussain, J.G. Körner, G. Thompson, MZ-TH-92-22 (1992).
28. N. Isgur and M. Wise, Phys. Rev. **D43** 819 (1991).
29. J. Bjorken, invited talk at Les Rencontre de Physique de la Vallee d'Aoste, La Thuile, Italy. SLAC Report No. SLAC-PUB-5278, (1990) (unpublished).